Control of MHD Instabilities in the STOR-M Tokamak using Resonant Helical Coils

C. Xiao 1), S. Elgriw 1), D. Liu 1), D. Trembach 1), T. Asai 2), A. Hirose 1)

1) Plasma Physics Laboratory, University of Saskatchewan, Saskatoon, Canada
2) Department of Physics, Nihon University, Tokyo, Japan
E-mail contact of main author: chijin.xiao@usask.ca

Abstract. The resonant interaction between magnetohydrodynamic (MHD) instability modes and an externally applied helical magnetic field has been investigated in the Saskatchewan Torus-Modified (STOR-M) tokamak. The study has been carried out numerically using a 2D MHD equilibrium code and also experimentally using an $l = 2/n = 1$ helical coils through which a DC current pulse is applied during normal Ohmic discharge. It has been found numerically that the helical current can effectively suppress the resonant ($m = 2$, $n = 1$) magnetic islands when the value of safety factor at the plasma edge is relatively low (≤ 4). Also, it has been found numerically that (2, 1) islands with disruptive nature may be induced when the applied current exceeds a certain limit. Experimentally, significant suppression in the (2, 1) tearing mode fluctuations has been observed during the application of resonant field on STOR-M discharges. The suppression of (1, 1), (3, 1) and (4, 1) mode perturbations has been also observed. Furthermore, the resonant field induced a phase with reduced H_α radiation level, reduced loop voltage, and increased soft x-ray (SXR) emission.

1. Introduction:

It has been found in many tokamaks that resistive tearing MHD instabilities are responsible for different types of disruptions in the plasma. The minor disruptions may destabilize and degrade plasma confinement, while the major disruptions can terminate a plasma discharge [1]. MHD instabilities grow on resonant magnetic surfaces with rational values of the safety factor q. The fluctuations associated with MHD instabilities in the STOR-M tokamak, such as Mirnov oscillations and sawtooth oscillations, have been monitored and analyzed by a set of diagnostics and data processing techniques. Those fluctuating signals are characterized by temporal evolution and spatial structures characterized by the poloidal and toroidal fluctuation modes (m, n).

It has also been observed in tokamaks that the major disruptions are likely caused by the (2, 1) magnetic islands. Those disruptions can be either delayed or activated by means of resonant helical coils (RHCs) [2]. The resonant helical field (RHF) induced by RHCs can strongly influence the magnetic islands on $q = 2$ resonance surface in tokamaks, leading to more stable plasma discharges when RHCs are fed with small DC currents (typically 1 to 3 % of the plasma current). RHF can effectively reduce the width of magnetic islands and, hence, suppress the Mirnov oscillations. It should be noted that the applied helical current (I_{RHC}) has a threshold and exceeding this threshold results in plasma disruption. This disruption has no characteristic differences from that caused by disruptive instabilities.

Discrete Mirnov coils can measure the fluctuations of magnetic field associated with rotating magnetic islands, and SXR photodiodes monitor the change of SXR emissivity in the magnetic islands. The MHD modes (m, n) are monitored in the STOR-M tokamak by arrays of discrete Mirnov coils mounted at various poloidal and toroidal locations. The Mirnov arrays have been complemented with an SXR detection system with two photodiode arrays. The time-resolved frequency analysis of transient and non-stationary fluctuating signals has been performed using the Morlet wavelet function. Frequencies and mode numbers, corresponding to

the temporal evolutions and spatial structures of the fluctuating MHD modes have been extracted using the Fourier coefficient decomposition (FCD) [3], and the singular value decomposition (SVD) algorithm [4].

This paper is organized as follows. Section 2 describes the layout of RHC, Mirnov coils and SXR cameras installed in STOR-M. Section 3 presents the results of RHC simulation using a 2D, fixed boundary Grad-Shafranov solver (TOSCA code) [5] to determine the critical I_{RHC} for different STOR-M discharge conditions. Section 4 discusses the analyses and experimental results, particularly through comparison among the features of magnetic fluctuations before, during and after applying I_{RHC}. Discussion of results and conclusions are given in Sec. 5.

2. Experimental Setup

STOR-M is a small research tokamak located at the University of Saskatchewan [6]. It has a major radius of 46 cm and minor radius of 12 cm. STOR-M is equipped with a real-time feedback position controller unit for the plasma horizontal position. The tokamak is equipped with four poloidal arrays of the discrete Mirnov coils, which are used to detect magnetic MHD oscillations. Two poloidal arrays, each consisting of 12 discrete Mirnov coils with a poloidal separation of 30°, are toroidally separated by 180°, and mounted on thin stainless steel bellows with a thickness of 0.5 mm. The spatial resolution of the arrays can resolve poloidal mode numbers up to $m = 6$. The toroidal modes are determined using four set of toroidal arrays, each including 4 discrete Mirnov coils toroidally separated by 90°. The outboard toroidal array is often used to measure the toroidal mode numbers up to $n = 2$.

An SXR system consisting of two miniature pin-hole cameras has been installed on STOR-M [7]. Each camera consists of a 20-channel photodiode linear array (IRD AXUV-20EL) of which only 12 are actually used. The SXR emissions are collected from 12 fan-like lines of sight. The visible light is filtered out using aluminum foils with a thickness of 1.8μm although a small peak in the 10-90 eV range exists in the transmission curve. The SXR cameras have been installed through horizontal and vertical ports poloidally separated by 90°, but located at the same toroidal angle. The signals of both Mirnov coils and SXR cameras are collected by a 14-bit digitizer with a maximum sampling rate of 3 MS/s per channel. Figures 1(a) and 1(b) show a schematic distribution of the discrete Mirnov coils and the vertical and horizontal lines of sight of SXR cameras.

Resonant helical field (RHF) is produced by a current pulse I_{RHC} driven in opposite directions through two sets of helical coils with $l = 2/n = 1$ windings installed outside the stainless vacuum chamber with a thickness of 4 mm. The current pulse is generated using a 25mF, 450V capacitor bank and gated by a 600A, 1400V IGBT switch. The current limit for the IGBT can be exceeded in the pulsed operation mode. The coils wound around the vacuum chamber are poloidally separated by 90° as shown in Fig. 1(c). In order to achieve resonant interaction between RHF and (2, 1) magnetic islands, the coils have to be configured in a way that their helicities (or the pitch angles) match the helicity of (2, 1) perturbations. When the MHD perturbations and the helical coils have opposite helicities, the resonant interaction does not occur [8]. The helicity of MHD perturbations is defined by the directions of I_p and B_φ. In STOR-M, the direction of I_p is counter clockwise, whereas B_φ is clockwise, resulting in MHD perturbations with helicity similar to that of RHC (the solid black lines in Fig. 1(c)).

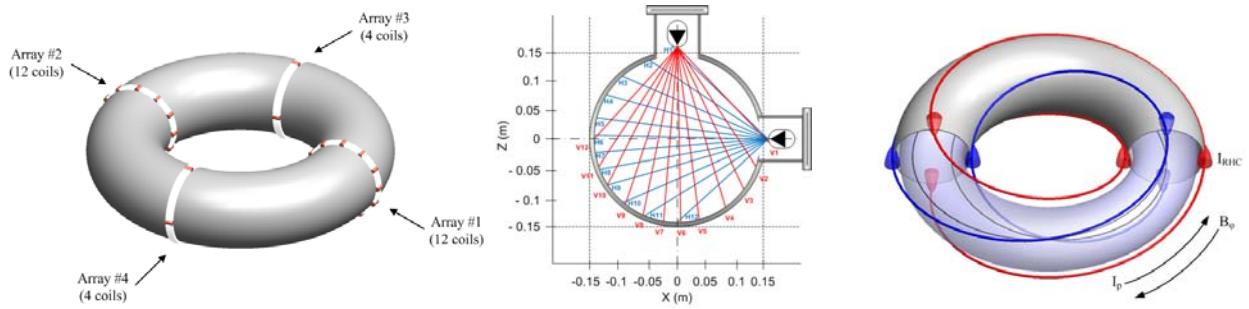

(a) (b) (c)

FIG. 1. (a) Distribution of Mirnov coil array, (b) lines of sight of SXR cameras and (c) the configuration of RHCs in STOR-M tokamak.

3. RHF Simulation

A numerical simulation has been performed for different scenarios of STOR-M equilibrium for actual STOR-M dimensions (minor radius of a = 0.12 m and major radius of R = 0.46 m). A 2D, fixed boundary Grad-Shafranov code, called TOSCA code, has been used to calculate the poloidal magnetic flux surfaces. The code also calculates the Shafranov shift as well as the safety factor q for each surface. A supplementary MATLAB code has been developed to impose magnetic perturbations on the q = 2 resonance surface, simulating an m = 2 magnetic island. The magnetic perturbations are expressed by $\varphi_{mn} = -\sum_{m,n} \alpha_{mn} q e^{i(n\varphi - m\theta)}/(m - nq)$, where m and n are the poloidal and toroidal mode numbers, and α_{mn} is a numerical factor impacting the island width. The perturbations are calculated for an island with m = 2, n = 1 and $\alpha_{21} = 0.25 \times 10^{-6}$. The MATLAB code has also been used to model RHC by four toroidal current conductors with a square cross-section of 25 mm^2. The coils located at poloidal angles 45° and 225° carry negative currents, while the ones located at 135° and 315° carry positive currents. The coils are placed at 17 cm from the plasma center. Two cases have been considered in this simulation, both with the same poloidal beta β_p (= 0.5) and B_φ (= 0.575 T) but with different plasma currents I_p (22.5 kA and 25 kA). The corresponding edge safety factors $q(a)$ for the two cases are 4 and 3.6, respectively.

The first case considered in the numerical simulation was a discharge with I_p = 22.5 kA, B_φ = 0.575 T and $q(a)$ = 4. At equilibrium (no I_{RHC} applied), the m = 2 island, shown in Fig. 2(a), has a width of 0.2 cm and radius of 7.3 cm. The distance between the island and RHC is approximately 9.7 cm. As shown in Fig. 2(b), the island width decreases by half (0.1 cm) when I_{RHC} increases from 0 A to 725 A. The island completely vanishes (Fig. 2(c)) when I_{RHC} reaches a critical value of 1450 A, which corresponds to 6.4 % of the plasma current I_p. As mentioned earlier, exceeding the critical I_{RHC} would trigger a disruptive m = 2 instability. This can be clearly seen in Fig. 2(d). As I_{RHC} increases to 2175 A, an m = 2 magnetic island is formed with a width of 0.1 cm. Increasing I_{RHC} even further would aggravate the island which may eventually lead to a major disruption in a plasma discharge as observed previously in other tokamaks (e.g., the TBR-1 tokamak) [9].

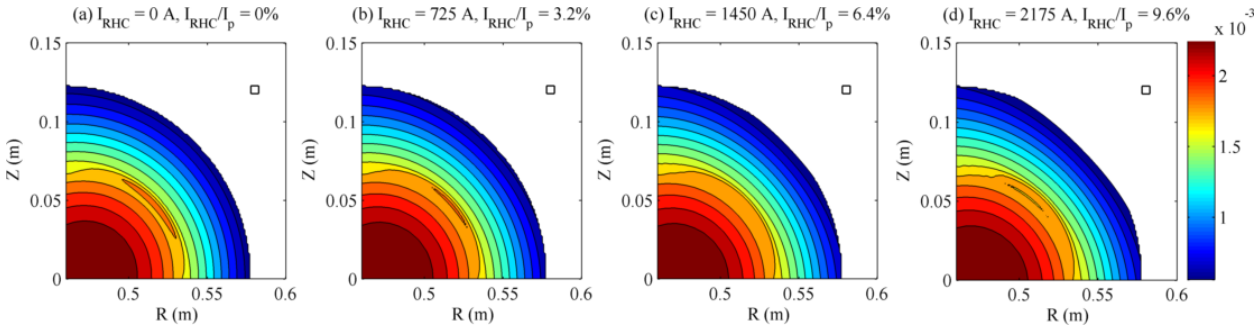

FIG. 2. Effect of RHC current on an m = 2 magnetic island during a STOR-M discharge with I_p = 22.5 kA, B_φ = 0.575 T and q(a) = 4.

Based on the simulation results for $q(a)$ = 4 tokamak discharge, it is expected that lowering the safety factor $q(a)$ will also lower the critical value of I_{RHC}. However, in STOR-M, q-value at the plasma edge should be kept above 3 to avoid deterioration in confinement time and large helical magnetic field perturbations. In another numerical simulation, the plasma current I_p has been increased to 25 kA, providing that $q(a)$ = 3.6 when B_φ = 0.575 T. The m = 2 island shown in Fig. 3(a) is now located at a distance of 8.5 cm from the plasma center. The width of island is roughly 0.2 cm in the absence of I_{RHC}. Increasing I_{RHC} gradually from 0 A to 550 A decreases the island width from 0.2 cm to 0.1 cm as illustrated in Fig. 3(b). It should be pointed out that in the previous case, a higher I_{RHC} (about 725 A) was required to reduce the m = 2 island width by 0.1 cm. Figure 3(c) shows a complete suppression of the m = 2 island when the I_{RHC} magnitude reaches a critical value of 1100 A, which is about 4.4 % of the total plasma current. Suppressing the m = 2 island with lower I_{RHC} is an expected result as the distance between the q = 2 surface and RHCs (8.5 cm) is smaller compared to the previous case (9.7 cm). When I_{RHC} increased to a value of 1650 A, a new m = 2 island with a width of 0.1 cm is produced (shown in Fig. 3(d)).

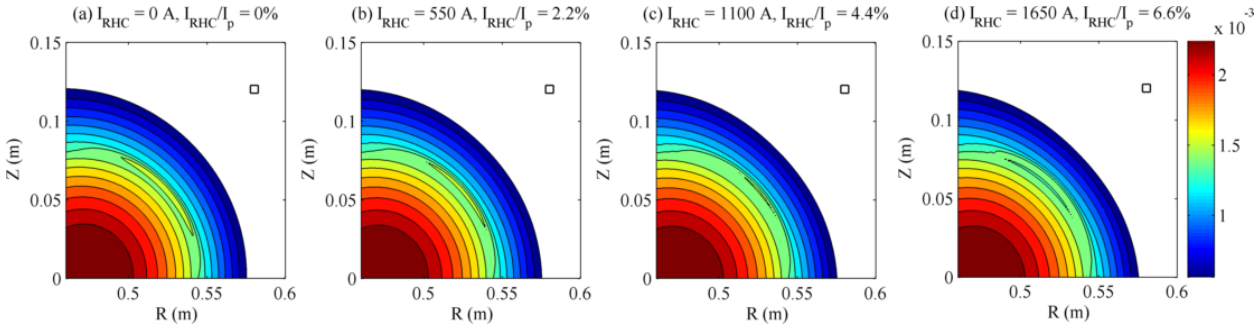

FIG. 3. Effect of RHC current on an m = 2 magnetic island during a STOR-M discharge with I_p = 25 kA, B_φ = 0.575 T and q(a) = 3.6.

4. Experimental Results

The influence of I_{RHC} on plasma parameters has been experimentally examined in STOR-M. During the discharge #225915, a current pulse of about 2 ms was applied during an MHD active phase. The discharge parameters shown in Fig. 4(a) are, from top, plasma current I_p, loop voltage V_l, horizontal plasma position ΔH, H_α radiation, edge safety factor $q(a)$, SXR emission

and Mirnov fluctuations. In this discharge (I_p = 23.5 kA, V_l = 3.5 V, $q(a)$= 3.7), I_{RHC} pulse was applied at 20 ms during the flattop plasma current for a duration of 2 ms. The amount of current driven in RHC is about 600 A (2.5% of total plasma current). Flatness in plasma current and loop voltage traces with slight reduction in H_α emission level (~40%) occur approximately 0.7 ms after the start of I_{RHC}. The plasma column is shifted by 3 mm in the outward direction. The main effect of I_{RHC} on the discharge is the significant suppression in MHD fluctuation signal and enhanced SXR emission from the plasma core. Figure 4(b) shows the three expanded waveforms of I_{RHC}, central SXR signal and Mirnov fluctuation signal. The negative peak in I_{RHC} is an artefact due to fast change in the current when the IGBT is switched off. The amplitude of MHD oscillations is strongly attenuated between 20.7 ms and 22 ms. However, the MHD activities resume oscillating at the initial frequency and amplitude when I_{RHC} is turned off.

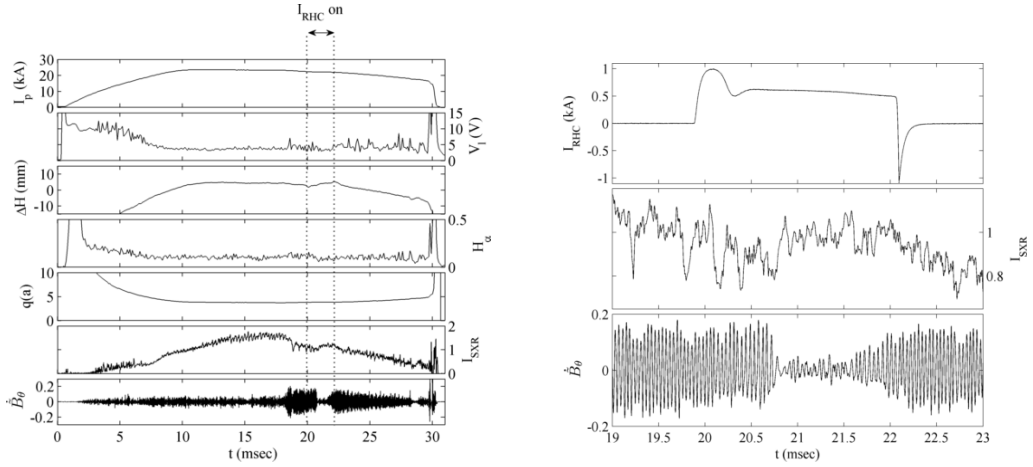

(a) (b)

FIG. 4. Resonant effect of I_{RHC} on plasma parameters during STOR-M discharge #225915. The resonant field was applied at 20 ms for about 2 ms during plasma current plateau.

Figure 5(a) shows expanded traces of Mirnov and SXR signals around the time of firing I_{RHC}. The traces shown in this figure are signals from two central SXR chords V7 and V8 (see Fig. 1(b)) and from an inboard magnetic probe. Clear sawtooth and inverted sawtooth can be seen in V7 and V8 signals respectively. Sawtooth oscillations are usually active when the relative amplitude of Mirnov signals is low during the period from 15 ms to 18 ms. However, the sawtooth oscillations vanish when Mirnov oscillations start growing at 18 ms. During the high Mirnov amplitude phase, the oscillations imposed on SXR signals are found to be well correlated with Mirnov oscillations (refer to Fig. 5(b)). The helical current applied at 20 ms causes a strong decay in Mirnov amplitude and an increase in the averaged SXR level in the V7 channel.

Figure 5(b) shows Morlet wavelet spectra of Mirnov and SXR signals. Both signals are clearly coherent at a frequency of 25kHz before and after applying I_{RHC}. However, during the I_{RHC} pulse, a gradual reduction in MHD amplitude and frequency can be seen on Mirnov spectrum between 20 ms and 20.7 ms. The MHD frequency is reduced from 25 kHz to 20kHz. This reduction in amplitude and frequency is missing on SXR spectrum since the m = 2 oscillations on the SXR signal reduced to an undetectable level immediately following the application of the RHF. The difference in the responses of SXR and Mirnov signals to RHF seems to suggest that the temperature peaks in the island disappears event before the island magnetic field structure vanishes.

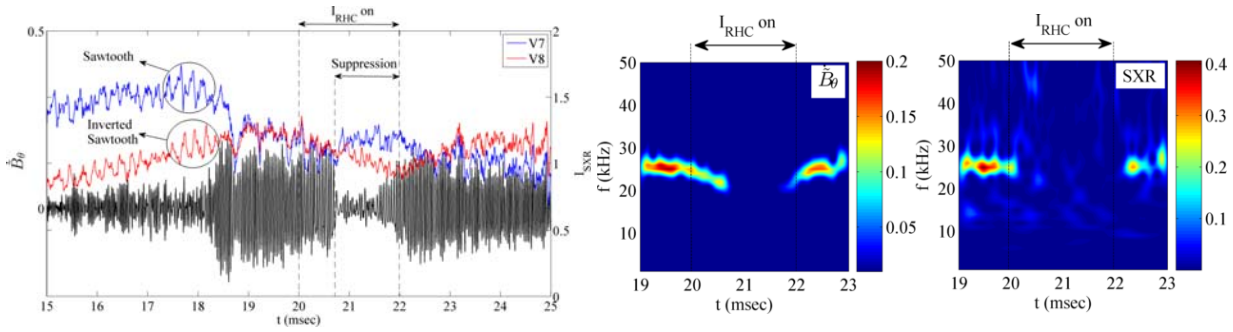

(a) (b)

FIG. 5. (a) Expanded traces of Mirnov and SXR signals and (b) comparison between the effect of I_{RHC} on Mirnov and SXR signals using wavelet power spectra. Mirnov and SXR are highly coherent at 25 kHz before and after I_{RHC} pulse.

The spatial structure of MHD modes before applying I_{RHC}, during MHD suppression and after turning off I_{RHC} has been extracted using the SVD analysis. Three time windows, each 0.5 ms long, have been chosen for the SVD analysis. The windows are located before (19.5-20ms), during (21-21.5ms) and after (22.25-22.75ms) applying I_{RHC}. SVD can extract the spatial features of MHD modes in a form of eigenvectors called principal axes (PAs). PAs of the dominant poloidal MHD modes before, during and after the I_{RHC} pulse are respectively shown in polar plots in Fig. 6(a), (b) and (c). Figure 6(b) corresponds to the dominant mode during the MHD suppression. The spatial structure can be clearly identified as an m = 3 mode. The modes shown in Fig. 6(a) and Fig. 6(c) are spatially distorted, although they have a similar structure. The distortion in PA indicates that two or more modes oscillating at the same frequency (i.e. mode coupling). The coupled MHD harmonics can be identified by performing a spatial Fourier analysis on the distorted PA. The toroidal mode number corresponds to n = 1 in this discharge, which is the typical case for most of STOR-M discharges.

Figure 6(d) shows relative mode spectra of PAs as extracted by the Fourier analysis. The spectrum of first PA (before firing I_{RHC}) shows that the coupled mode comprised mainly of m = 2 mode (~52%) and m = 3 mode (~26%). Other modes (i.e. m = 1 and m = 4 modes) also appear in the spectrum with no significant contribution to the global mode amplitude. During the MHD suppression phase (21-21.5ms), the mode spectrum indicates that the dominant poloidal number is m = 3 with energy content up to 54%. Although m = 2 also contributes to the spectrum by 23%, it does not distort the spatial structure of the dominant m = 3 mode as shown in Fig. 6(b). After turning off I_{RHC}, the m = 2 mode grows again causing a spatial distortion to the dominant mode, similar to the case before applying I_{RHC}. The m = 2 mode oscillates with a relative amplitude of 48%, while the m = 3 mode oscillates with an amplitude of 28%. Apparently I_{RHC} does not have a strong effect on m = 1 and m = 4 modes since they maintain the same relative amplitude in the three cases. Note that the plots are percentage amplitudes normalized for signals within each time window. Comparison of the absolute amplitudes of any particular mode for three time windows cannot be extracted from Fig. 6(d).

The magnitude of harmonics from m = 1 to m = 4 modes can be obtained using FCD. FCD is a numerical method based on spatial Fourier series and which decomposes the sine and cosine components of each mode from raw Mirnov signals. The analysis was performed on the time segment 19-23 ms (1 ms before and after applying I_{RHC}). The FCD magnitudes are plotted in Fig. 7(a). Clearly the m = 2 mode has the highest magnitude among the other modes before firing the I_{RHC} pulse. There is no visible change in mode magnitudes for about 0.7 ms from

applying the helical current. However, the m = 2 magnitude drops suddenly by 90% at 20.7 ms, while the other modes are suppressed by approximately 65-75%. The m = 3 fluctuation amplitude dominates over the other modes during the suppression phase. The suppression lasts for about 1.5 ms until t = 22 ms when the modes start oscillating at their original amplitudes prior to applying I_{RHC}, with m = 2 being the dominant mode again. The noise spike on the figure at 22 ms is caused a spike in I_{RHC} when the current is suddenly turned off by the IGBT switch as shown in Fig. 4(b). The spike appears on some Mirnov signals when the coil is close RHC winding, but it does not show up on other diagnostic signals (see Fig. 4(a)). This spike will be compensated for in the future RHF experiments.

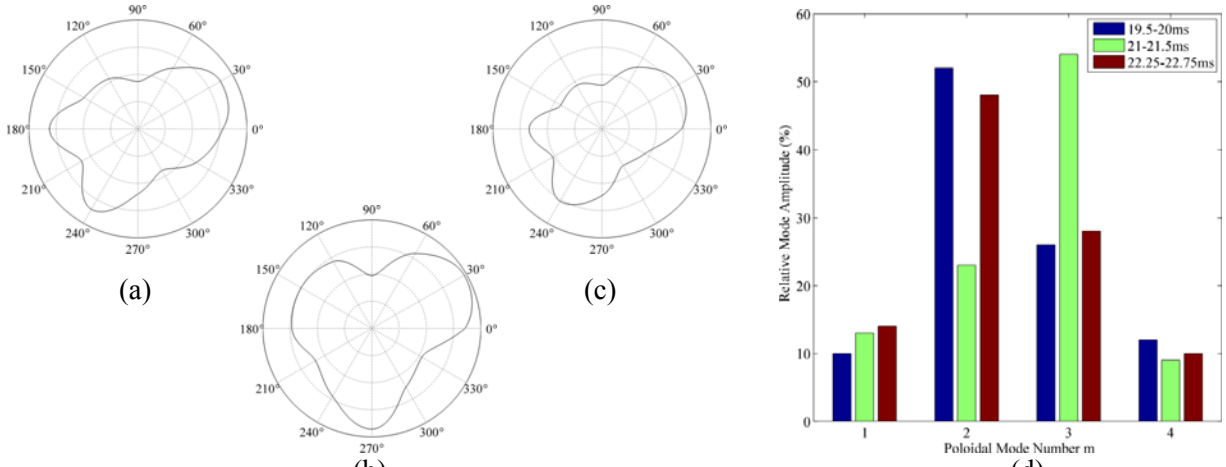

FIG. 6. Spatial structure of dominant poloidal MHD modes (a) before (b) during and (c) after applying I_{RHC} as extracted by SVD and (d) the corresponding Spatial Fourier analysis.

Figure 7(b) shows three radial profiles of SXR emissivity constructed at 19.84 ms, 21.96 ms and 22.74 ms. The profiles at 19.84 ms and 22.74 ms, located before and after applying I_{RHC}, have a similar radial distribution centered around V8 channel. However, during the I_{RHC} pulse (21.96 ms), high SXR emission level is observed by V4 channel. In addition, the radial SXR brightness profile shifts outward along with the plasma displacement ΔH.

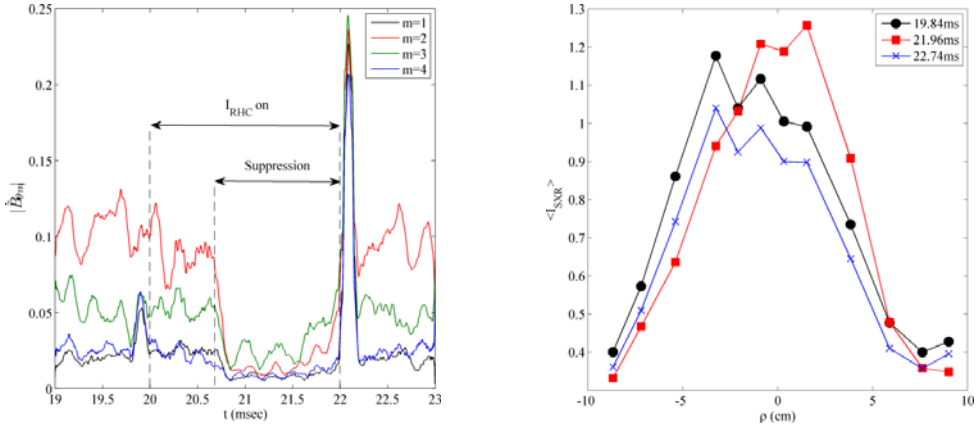

(a) (b)

FIG. 7. (a) Mode magnitudes for MHD modes up to m = 4 and (b) radial profiles of SXR intensity around the time of firing I_{RHC}.

5. Conclusions:

It has been reported in many tokamaks that the behaviour of MHD perturbations can be controlled by means of resonant magnetic fields generated by external helical windings. An numerical simulation has been carried out for two equilibrium states of STOR-M for different RHC currents and edge safety factors. RHF showed a significant effect on an $m = 2$ island superimposed on $q = 2$ surface. The island has been reduced or even eliminated by RHF when $q(a)$ was near 4. The amount of helical current used was about 6.4% of the plasma current. Reducing $q(a)$ to 3.6 decreased the amount of current required to suppress the island to 4.4% of I_p. When the helical current exceeded a critical limit, an island with $m = 2$ structure has been reproduced which may be responsible for the reported disruptive instability.

Effects of RHF have been studied in STOR-M during a typical ohmic discharge (I_p = 23.5kA, V_l = 3.5V, $q(a)$= 3.7). The I_{RHC} pulse (~2.5% of I_p) has been applied during plasma plateau phase with strong Mirnov activities. Reduction in loop voltage V_l and in H_α emission level has been observed 0.7 ms after firing I_{RHC}. Mirnov oscillations were dramatically suppressed and the MHD rotating frequency reduced. The amplitude of $m = 2$ mode dropped by about 90%, while by 65-75% for the other modes. The $m = 3$ mode was dominant during the MHD suppression phase before the $m = 2$ oscillations dominated the discharge again when I_{RHC} was turned off. The SXR oscillations were strongly coherent with Mirnov oscillations at a frequency of 25 kHz before and after applying I_{RHC}. The MHD frequency was reduced from 25kHz to 20kHz during the suppression phase. High SXR emissivities were observed by central SXR chords when the MHD modes were suppressed.

Acknowledgements

The authors would like to thank D. McColl for his technical assistance. This work was sponsored by the Natural Sciences and Engineering Research Council of Canada (NSERC) and Canada Research Chair (CRC) program.

References:

[1] A. I. Morozov and L. S. Solovev, *The Structure of Magnetic Fields, In Reviews of Plasma Physics 2*, Consultants Bureau New York (1966).
[2] F. Karger, H. Wobig, S. Corti *et al.*, in *Plasma Physics and Controlled Nuclear Fusion Energy Research 1974, IAEA Proc. 5th Int. Conf.* **1**, 207 (1975).
[3] J. S. Bendat and A. G. Piersol, *Engineering Applications of Correlation and Spectral Analysis 2nd Ed*, John Wiley and Sons Inc. (1993).
[4] C. Nardone*, Plasma Phys. Control. Fusion* **34**, 1447 (1992).
[5] K. Shinya, , *Journal of Plasma and Fusion Research* **76**, 479 (2000).
[6] A. Hirose, C. Xiao, O. Mitarai, J. E. Morelli and H. Skarsgard, *Physics in Canada* **62**, 111 (2006).
[7] C. Xiao, T. Niu, J. E. Morelli, C. Paz-Soldan, M. Dreval, S. Elgriw, A. Pant, D. Rohraff, D. Trembach and A. Hirose, *Rev. Sci. Instrum.* **79**, 10E926 (2008).
[8] D. E. Roberts, D. Sherwell, J. D. Fletcher *et al., Nucl. Fusion* **31**, 319 (1991).
[9] M. S. T. Araújo, A. Vannucci and I. L. Caldas*, Il Nuovo Cimento D* **18**, 807 (1996).